







Article

Galeite, $\text{Na}_{15}(\text{SO}_4)_5\text{ClF}_4$, and Schairerite, $\text{Na}_{21}(\text{SO}_4)_7\text{ClF}_6$: Phase Transitions, Thermal Expansion and Thermal Stability

Margarita S. Avdontceva ^{1,*} , Andrey A. Zolotarev ¹ , Andrey P. Shablinskii ² , Vladimir N. Bocharov ³ , Anatoly V. Kasatkin ⁴  and Sergey V. Krivovichev ^{1,5} 

¹ Institute of Earth Sciences, St. Petersburg State University, University Emb. 7/9, St. Petersburg 199034, Russia

² Institute of Silicate Chemistry of the Russian Academy of Sciences (ISC RAS), Makarova Emb. 2, St. Petersburg 199034, Russia

³ Centre for Geo-Environmental Research and Modelling, St. Petersburg State University, University Emb. 7/9, St. Petersburg 199034, Russia

⁴ Fersman Mineralogical Museum, Russian Academy of Sciences, Leninskiy Prospect 18-2, Moscow 119071, Russia

⁵ Nanomaterials Research Centre, Kola Science Center, Russian Academy of Sciences, Fersmana Str. 14, Apatity 184209, Russia

* Correspondence: m.avdontceva@spbu.ru

Abstract: In this study, galeite, $\text{Na}_{15}(\text{SO}_4)_5\text{ClF}_4$ and schairerite, $\text{Na}_{21}(\text{SO}_4)_7\text{ClF}_6$ were investigated via in situ single-crystal X-ray diffraction in the temperature range of 300–750 K. Galeite and schairerite are trigonal, $P31m$, $a = 12.1903(2)$, $c = 13.9454(2)$ Å, $V = 1794.69(6)$ Å³, and $Z = 3$ ($R_1 = 0.0273$, 300 K) for galeite and $a = 12.1859(3)$, $c = 19.3080(6)$ Å, $V = 2483.04(14)$ Å³, and $Z = 3$ ($R_1 = 0.0334$, 300 K) for schairerite. The crystal structures of galeite and schairerite are based upon frameworks consisting of alternating face- and corner-sharing fluorine- and chlorine-centered octahedra. Galeite and schairerite can be attributed to $5H$ (galeite) and $7H$ (schairerite) antiperovskite polytypes, respectively. It was observed that schairerite undergoes at least one reversible phase transition before it starts to lose its crystallinity at 750 K. This phase transition occurs in the temperature range of 550–600 K. The high-temperature modification of schairerite is trigonal, with the centrosymmetric space group $P-3m1$ and the unit-cell parameters $a = 7.0714(2)$, $c = 19.5972(7)$ Å, $V = 848.66(6)$ Å³, and $Z = 1$. Galeite is stable up to 600 K. The crystal structures of minerals expand anisotropically, and, in both cases, the strongest thermal expansion was parallel to the modules of face-sharing anion-centered octahedra. The structural complexity analysis showed that galeite is complex (695.175 bits/cell) and that the LT-modification of schairerite is very complex (1064.990 bits/cell), whereas its HT-modification is intermediate in complexity (256.755 bits/cell). The complexities of LT- and HT-polymorphs of schairerite are consistent with the general observations regarding structures with positional disorder: complexity decreases with increasing temperature, and simpler polymorphs have lower physical density.

Keywords: galeite; schairerite; thermal evolution; phase transition; X-ray diffraction studies; complexity



Citation: Avdontceva, M.S.; Zolotarev, A.A.; Shablinskii, A.P.; Bocharov, V.N.; Kasatkin, A.V.; Krivovichev, S.V. Galeite, $\text{Na}_{15}(\text{SO}_4)_5\text{ClF}_4$, and Schairerite, $\text{Na}_{21}(\text{SO}_4)_7\text{ClF}_6$: Phase Transitions, Thermal Expansion and Thermal Stability. *Symmetry* **2023**, *15*, 1871. <https://doi.org/10.3390/sym15101871>

Academic Editor: Mikhail Sheremet

Received: 26 August 2023

Revised: 21 September 2023

Accepted: 25 September 2023

Published: 5 October 2023



Copyright: © 2023 by the authors. Licensee MDPI, Basel, Switzerland. This article is an open access article distributed under the terms and conditions of the Creative Commons Attribution (CC BY) license (<https://creativecommons.org/licenses/by/4.0/>).

1. Introduction

Galeite, $\text{Na}_{15}(\text{SO}_4)_5\text{ClF}_4$ and schairerite, $\text{Na}_{21}(\text{SO}_4)_7\text{ClF}_6$, rare sodium sulfates with additional F and Cl anions, are members of the Na_2SO_4 -NaF-NaCl system. This system also includes kogarkoite, $\text{Na}_3\text{SO}_4\text{F}$ [1,2] and sulphohalite, $\text{Na}_6(\text{SO}_4)_2\text{FCl}$, with the latter having a F:Cl ratio of 1:1 [3,4]. These minerals are of particular interest due to their antiperovskite-type crystal structures [5]. Generally, antiperovskites are compounds with crystal structures based on anion-centered octahedral networks, which distinguishes them from classical perovskites consisting of cation-centered octahedra. Inorganic compounds with antiperovskite structures demonstrate unique physical and chemical features such as superconductivity, luminescence, negative thermal expansion, etc. [6–10]. For instance, recent luminescence

studies of Eu-doped $\text{Na}_3\text{SO}_4\text{F}$ and NaMgSO_4F demonstrated that the PL-emission spectra of Eu^{3+} ions in $\text{Na}_3\text{SO}_4\text{F}:\text{Eu}$ and $\text{NaMgSO}_4\text{F}:\text{Eu}$ phosphors are applicable to the production of mercury-free lamps [11]. Inorganic oxysalts with antiperovskite structures possess some interesting phase transitions associated with order–disorder reactions (see our recent works on synthetic kogarkoite [12] and nacaphite [13]).

Galeite and schairerite were originally described in evaporates of Searles lake (California) [14–16]. Galeite has been predominantly found in drill cores of «lower salt» part in a variety of forms including pyramidal or barrel-shaped crystals, friable clusters or aggregates, polycrystals, and uncommonly tabular habit crystals, which are almost always associated with gaylussite, $\text{Na}_2\text{Ca}(\text{CO}_3)_2 \cdot 5\text{H}_2\text{O}$ or northupite, $\text{Na}_3\text{Mg}(\text{CO}_3)_2\text{Cl}$ [17]. Schairerite was originally described by Foshag [16] at an unspecified depth as tiny crystals up to 2 mm in diameter with inclusions of hanksite, $\text{KNa}_{22}(\text{SO}_4)_9(\text{CO}_3)_2\text{Cl}$. The crystals had various degrees of shape distortion, and some of them appeared as trigonal rhombs. Later, Pabst et al. [15] reported different types of schairerite crystals, including schairerite–galeite polycrystals.

According to its initial description and chemical data, it has been assumed that galeite is dimorphous with schairerite [14]. Pabst et al. [15] refuted this statement and revealed that these minerals have different F/Cl ratios, namely, 4:1 for galeite and 6:1 for schairerite, but the same diffraction symmetry $-31mP$. The authors also showed that the unit cells of galeite and schairerite can be related to the unit cells of sulphohalite described in a trigonal setting.

The crystal structures of schairerite and galeite were solved and refined by Fanfani and co-authors [18,19]. Both minerals were described as trigonal, with the $P31m$ space group ($a = 12.197$ and $c = 13.955$ Å for galeite ($R_1 = 0.09$) and $a = 12.197$ and $c = 19.259$ Å for schairerite ($R_1 = 0.07$)). The marked subcells with $P-3m1$ symmetry were identified for both minerals, with $a = 7.042$ Å and the c parameters as originally reported.

This work is a continuation of our previous studies devoted to the investigation of the crystal chemical features of antiperovskite minerals and their synthetic analogues under changing temperature conditions. Herein, we discuss the results of in situ single crystal X-ray diffraction studies of galeite and schairerite at different temperatures and present a calculation and comparison of their structural complexities and potential Na-ion transport [12,13,20,21].

2. Materials and Methods

2.1. Samples

The studied samples were obtained from the personal collection of Anatoly V. Kasatkin. Both specimens originate from the same locality (Searles lake (California)). Galeite and schairerite were represented by four transparent, colorless single crystals of different sizes and forms: two near-spherical crystals of galeite up to 0.1 mm in diameter (collection number 680 G) and two hexagonal plates of schairerite from 0.05 mm to 0.2 mm in diameter (with collection numbers 865 h and 180 Sh, respectively) (Figure 1).

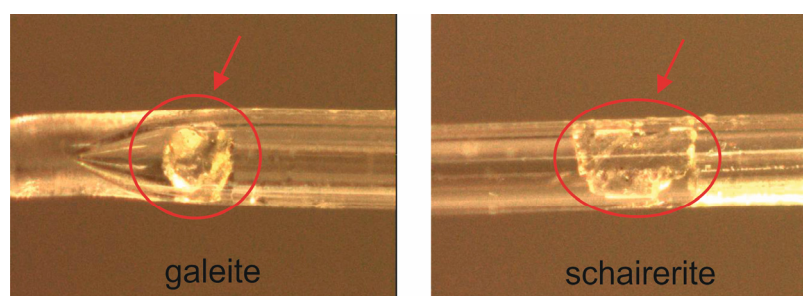


Figure 1. The crystals of galeite and schairerite (circled in red) fixed in quartz capillaries (for more details, see Section 2.2).

2.2. X-ray Diffraction Data

The thermal behavior of galeite and schairerite was studied via in situ single-crystal X-ray diffraction analysis using a Rigaku XtaLAB Synergy-S diffractometer (MoK α radiation, 50 kV and 1.0 mA) equipped with a high-speed direct-action detector (HyPix-6000HE). The heating process was controlled using a «Hot Air gas blower» system. The crystals of galeite and schairerite were placed and fixed in quartz capillaries with an approximately 10-micron wall thickness. The hemispheres of diffraction data (with a frame width of 0.5°) were collected for each temperature. The counting times were 2.0 (galeite) and 2.5 s (schairerite) for each frame, respectively. The orientation of the crystals did not change during all measurements. The CrysAlisPro software was used for data processing [22]. An absorption correction was introduced using the SCALE3 ABSPACK algorithm [23]. The crystal structures were determined and refined using the SHELX program package intercalated in the Olex2 shell [24].

Schairerite was studied at a temperature range from 300 to 750 K with a step of 50 K. It was observed that schairerite underwent at least one reversible phase transition before it started to lose its crystallinity at 750 K. This phase transition occurs in the temperature range of 500–600 K. The high-temperature modification of schairerite (HT) is trigonal, with the centrosymmetric space group $P\bar{3}m1$ and the following unit cell parameters: $a = 7.0714(2)$, $c = 19.5972(7)$ Å, and $V = 848.66(6)$ Å³. In the X-ray diffraction patterns collected at 500–550 K, the appearance of additional reflections with extremely weak intensity was observed, which led to an intermediate phase with a doubled value of parameter a compared to the HT modification ($a = 14.1171(4)$, $c = 19.4762(6)$ Å, and $V = 3361.44(17)$ Å³ at 550 K). The attempts to refine the crystal structure with these unit cell parameters were unsuccessful and led to high R values, whereas the refinement with the high-temperature model ($a = 7.0634(2)$, $c = 19.5290(6)$ Å, and $V = 843.80(4)$ Å³) allowed for the refinement of the crystal structure to $R_1 = 0.044$ at 550 K. We attribute the additional reflections to the intermediate state transition between the low- and high-temperature modifications and posit that they were most likely due to the overlapping of domains corresponding to the upcoming HT phase.

These changes can clearly be identified through the analysis of the reconstructed reciprocal space obtained for ($hk0$) sections (Figure 2). The relations between unit cells are shown in Figure 3.

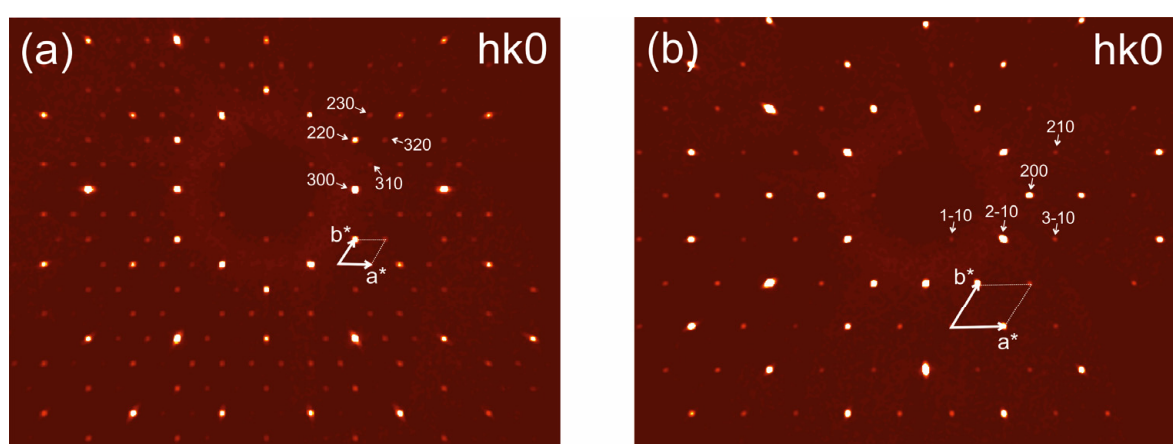


Figure 2. Reconstructed sections of reciprocal diffraction space for low-temperature (300 K) (a) and high-temperature (600 K) (b) modifications of schairerite, the projection of $hk0$ plane. The arrows and dotted lines correspond to the reciprocal lattices of the two modifications.

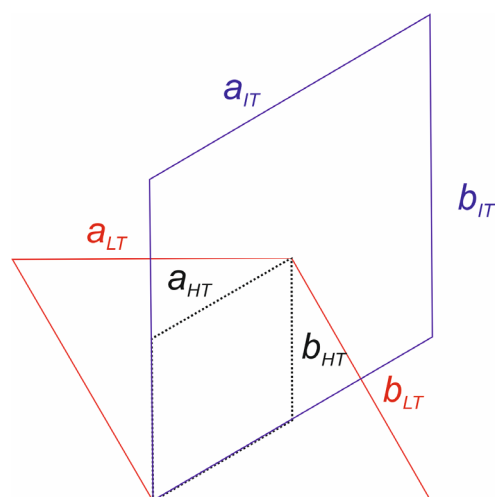


Figure 3. Relations between unit cells: low-temperature modification of schairerite (LT) is shown in red, intermediate phase (IT) is shown violet, and high-temperature phase (HT) is indicated by the black, dotted line.

Galeite was studied using two crystals in the temperature range of 300–700 K with a step of 100 K and from 300 K to 500 K with a step of 25 K. The investigation of the first crystal showed that its quality began to deteriorate at 600 K, progressing until the complete loss of crystallinity at 750 K. No phase transitions were observed. However, our detailed inspection of the reciprocal space at 600 K allows us to suggest that the correct unit cell parameters at this temperature are $a = 7.0812(3)$, $c = 14.5556(7)$ Å, and $V = 614.72(5)$ Å³, despite the low level of indexing (39%) and the high R_{int} value of 0.12 (Figure 4). The second crystal was studied for the sake of the high-quality measurement of the thermal expansion of the crystal structure.

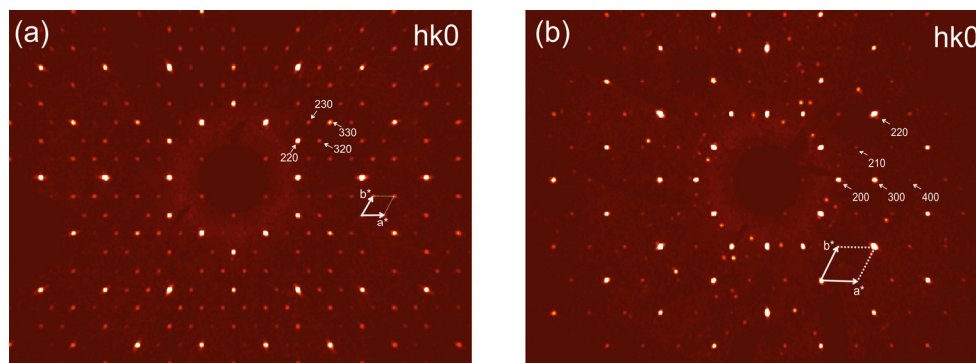


Figure 4. Reconstructed sections of the reciprocal space obtained for galeite at 300 K (a) and at 600 K (b) (the projection of $hk0$ plane). The arrows and dotted lines correspond to reciprocal lattices.

The following formula [25] of the rigid-body motion correction was used for all bond lengths in the crystal structures of galeite and schairerite

$$L^2 = l_0^2 + 3/8\pi^2(B_{eq}(A_2) - B_{eq}(A_1)), \quad (1)$$

where L and l_0 are corrected and observed A_1 – A_2 bond lengths, respectively. $B_{eq}(A_1)$ and $B_{eq}(A_2)$ are equivalent temperature factors of cations (A_1) and anions (A_2).

The main thermal expansion coefficients for all temperatures were calculated and visualized using the TTT program package [26]. The Vesta software was used for the visualization of the crystal structure and the calculation of polyhedral volumes (Å³) [27].

The best refinement data were obtained for the samples heated at 300 K and 600 K (HT-schairerite). The crystal data and structure refinement parameters for galeite and both modifications of schairerite are given in Table 1; atomic coordinates and displacement parameters are provided in Table 2, Table 3, and Table 4, respectively; and selected bond lengths are presented in Tables 5–7.

Table 1. Crystal data and structure refinement parameters of galeite at 300 K (1) and schairerite at 300 K (2) and 600 K (3), respectively.

Sample	1	2	3
Crystal system	trigonal	trigonal	trigonal
Temperature (K)	300	300	600
Space group	<i>P31m</i>	<i>P31m</i>	<i>P-3m1</i>
<i>a</i> , Å	12.1903(2)	12.1859(3)	7.0714(2)
<i>c</i> , Å	13.9454(2)	19.3080(6)	19.5972(7)
Volume, Å ³	1794.69(6)	2483.04(14)	848.66(6)
<i>Z</i>	3	3	1
<i>D</i> _{calc} (g/cm ³)	2.600	2.617	2.553
μ /mm ^{−1}	0.992	0.973	0.946
<i>F</i> (000)	1374.0	1914.0	638.0
Radiation	Mo K α (λ = 0.71073)	Mo K α (λ = 0.71073)	Mo K α (λ = 0.71073)
2 Θ range for data collection/°	6.684 to 59.452	6.688 to 59.258	6.654 to 58.898
Index ranges	−16 ≤ <i>h</i> ≤ 17, −16 ≤ <i>k</i> ≤ 16, −12 ≤ <i>l</i> ≤ 18	−16 ≤ <i>h</i> ≤ 16, −16 ≤ <i>k</i> ≤ 14, −26 ≤ <i>l</i> ≤ 24	−9 ≤ <i>h</i> ≤ 9, −9 ≤ <i>k</i> ≤ 9, −26 ≤ <i>l</i> ≤ 25
Reflections collected	19,614	20,070	8548
Independent reflections	2880 [<i>R</i> _{int} = 0.0215, <i>R</i> _{sigma} = 0.0134]	4396 [<i>R</i> _{int} = 0.0200, <i>R</i> _{sigma} = 0.0200]	910 [<i>R</i> _{int} = 0.0231, <i>R</i> _{sigma} = 0.0125]
Data/restraints/parameters	2880/1/242	4396/1/334	910/2/96
Goodness-of-fit on <i>F</i> ²	1.031	1.009	1.018
Final <i>R</i> indexes [<i>I</i> ≥ 2 σ (<i>I</i>)]	<i>R</i> ₁ = 0.0273, <i>wR</i> ₂ = 0.0708	<i>R</i> ₁ = 0.0334, <i>wR</i> ₂ = 0.0954	<i>R</i> ₁ = 0.0485, <i>wR</i> ₂ = 0.1603
Final <i>R</i> indices (all data)	<i>R</i> ₁ = 0.0294, <i>wR</i> ₂ = 0.0722	<i>R</i> ₁ = 0.0434, <i>wR</i> ₂ = 0.1017	<i>R</i> ₁ = 0.0577, <i>wR</i> ₂ = 0.1697
Largest diff. peak/hole/e Å ^{−3}	0.72/−0.57	0.78/−0.41	1.03/−0.72
Flack parameter	0.39(8)	0.39(13)	−

Table 2. Atomic coordinates and equivalent isotropic displacement parameters (Å²) of galeite at 300 K.

Atom	<i>x</i>	<i>y</i>	<i>z</i>	<i>U</i> (eq)
S1	0	0.66363(6)	0.11620(9)	0.0087(2)
S2	0	0	0.31174(12)	0.0087(3)
S3	1/3	2/3	0.33306(9)	0.0090(3)
S4	0.66946(6)	0.66946(6)	0.52601(8)	0.0093(2)
S5	0	0	0.68577(12)	0.0105(4)
S6	0.66750(6)	0.66750(6)	0.90763(8)	0.0091(2)
S7	1/3	2/3	0.70621(8)	0.0105(3)
Na1	0.66985(10)	0.52321(12)	0.13605(10)	0.0170(3)
Na2	0.82338(14)	0.82338(14)	0.12299(12)	0.0181(4)
Na3	0.66774(10)	0.83978(12)	0.31750(12)	0.0164(3)
Na4	0.48437(13)	0	0.32004(14)	0.0167(4)
Na5	0.81942(13)	0	0.50393(12)	0.0178(4)
Na6	0.51553(10)	0.84941(11)	0.50896(11)	0.0159(3)
Na7	0.51271(13)	0	0.70187(13)	0.0180(4)
Na8	0.81655(11)	0.15069(11)	0.70600(10)	0.0157(3)
Na9	0.66381(9)	1.15442(11)	0.89960(11)	0.0172(3)
Na10	0.81055(13)	0	0.89099(12)	0.0175(4)
Cl1	2/3	1/3	0.03306(9)	0.0090(3)
Cl2	0	0	0.98833(15)	0.0159(3)

Table 2. Cont.

Atom	<i>x</i>	<i>y</i>	<i>z</i>	<i>U</i> (eq)
F1	0.68341(16)	0.68341(16)	0.23875(19)	0.0139(5)
F2	0.65040(16)	0	0.3891	0.0147(5)
F3	0.67313(13)	0	0.59979(19)	0.0136(5)
F4	0.65865(15)	0	0.8018(2)	0.0138(5)
O1	0	0.5510(2)	0.1554(2)	0.0179(6)
O2	0	0.6602(2)	0.0105(2)	0.0175(7)
O3	0.88681(18)	0.66572(16)	0.15031(16)	0.0176(5)
O4	0	0	0.2056(3)	0.0176(10)
O5	0.88612(19)	0	0.3463(2)	0.0191(5)
O6	0.32870(14)	0.77844(17)	0.29846(16)	0.0187(5)
O7	1/3	2/3	0.4387(3)	0.0159(8)
O8	0.55369(19)	0.55369(19)	0.4955(2)	0.0179(5)
O9	0.66738(15)	0.78158(17)	0.48839(17)	0.0178(4)
O10	0.6751(2)	0.6751(2)	0.6318(3)	0.0189(7)
O11	0	0	0.5803(3)	0.0225(11)
O12	0.8860(2)	0	0.7206(2)	0.0212(6)
O13	0.5535(2)	0.5535(2)	0.8719(2)	0.0195(6)
O14	0.66662(16)	0.78125(17)	0.87227(17)	0.0182(5)
O15	0.6680(2)	0.6680(2)	1.0136(2)	0.0197(7)
O16	0.44651(18)	0.78111(17)	0.67108(17)	0.0211(5)
O17	1/3	2/3	0.8115(3)	0.0234(9)

Table 3. Atomic coordinates and equivalent isotropic displacement parameters (\AA^2) of schairerite at 300 K.

Atom	<i>x</i>	<i>y</i>	<i>z</i>	<i>U</i> (eq)
S1	1/3	2/3	0.09451(19)	0.0121(6)
S2	0	0	0.1132(2)	0.0086(8)
S3	−1/3	−1/3	0.36657(19)	0.0152(7)
S4	0	0.33645(16)	0.25295(13)	0.0083(4)
S5	0	0	0.3824(2)	0.0090(8)
S6	0.33401(17)	0	0.52579(12)	0.0104(5)
S7	1/3	2/3	0.82540(18)	0.0124(6)
S8	0.33306(16)	1.33306(16)	0.68017(12)	0.0086(4)
S9	0.33050(16)	1.33050(16)	0.95430(13)	0.0100(5)
S10	0	0	0.8402(2)	0.0092(9)
Na1	−0.1729(3)	0.6671(4)	0.10356(19)	0.0179(5)
Na2	0	0.8177(3)	0.2402(2)	0.0145(10)
Na3	0	0.5154(3)	0.1016(2)	0.0150(8)
Na4	0.1520(2)	0.6678(2)	0.23492(17)	0.0170(7)
Na5	0	0.5180(3)	0.3829(3)	0.0144(9)
Na6	−0.1521(2)	0.6675(2)	0.38059(17)	0.0158(6)
Na7	0	0.8237(3)	0.5217(3)	0.0195(10)
Na8	0.1488(2)	0.6687(2)	0.5159(2)	0.0208(7)
Na9	0.1884(3)	0	0.6892(3)	0.0204(9)
Na10	0.3340(2)	0.1509(2)	0.82455(17)	0.0159(7)
Na11	0.4845(2)	0.1506(2)	0.96599(16)	0.0153(7)
Na12	0.4867(3)	0	0.8268(3)	0.0175(10)
Na13	0.4890(2)	0.1535(2)	0.6835(2)	0.0212(7)
Na14	0.1805(3)	0	0.9705	0.0163(10)
Cl1	1/3	2/3	0/5885(2)	0.0234(6)
Cl2	0	1.0000	0.6169(3)	0.0188(7)
F1	0	0.3487(4)	0.0523(3)	0.0181(12)
F2	0	0.6835(4)	0.1536(3)	0.0144(11)
F3	0	0.6617(4)	0.3061(3)	0.0147(10)

Table 3. Cont.

Atom	<i>x</i>	<i>y</i>	<i>z</i>	<i>U</i> (eq)
F4	0	0.6739(4)	0.4515(3)	0.0125(10)
F5	0.3404(4)	0	0.7535(3)	0.0199(12)
F6	0.3271(4)	0	0.9013(3)	0.0125(10)
O1	1/3	2/3	0.0168(5)	0.0181(12)
O2	0.2218(3)	0.67111(19)	0.1172(3)	0.0214(10)
O3	−0.1136(4)	0.8864(4)	0.0872(3)	0.0233(12)
O4	0	0	0.1899(6)	0.0233(12)
O5	−1/3	1/3	0.2887(5)	0.032(2)
O6	−0.2209(4)	0.4476(4)	0.3902(3)	0.0245(13)
O7	−0.1151(4)	0.2198(4)	0.2297(3)	0.0199(12)
O8	0	0.4493(4)	0.2246(5)	0.0199(18)
O9	0	0.3403(5)	0.3297(4)	0.0186(13)
O10	0	0.8866(5)	0.3584(4)	0.0282(19)
O11	0	0	0.4585(6)	0.025(2)
O12	0.2197(4)	0.8866(4)	0.4996(3)	0.0243(13)
O13	0.4469(5)	0	0.4990(5)	0.0224(19)
O14	0.3344(6)	0	0.6001(4)	0.0257(15)
O15	1/3	2/3	0.7482(5)	0.027(12)
O16	0.3347(3)	0.7817(3)	0.8497(3)	0.0187(10)
O17	0.3319(5)	0.3319(5)	0.6026(4)	0.0192(13)
O18	0.3336(5)	0.2192(4)	0.7061(3)	0.0209(12)
O19	0.4468(4)	0.4468(4)	0.7056(5)	0.0198(18)
O20	0.3254(5)	0.3254(5)	0.8782(4)	0.0192(14)
O21	0.4446(4)	0.4446(4)	0.9772(4)	0.0165(16)
O22	0.3322(4)	0.2190(4)	0.9815(3)	0.0156(10)
O23	0	0	0.9170(6)	0.027(3)

Table 4. Atomic coordinates, occupancy factors, and equivalent isotropic displacement parameters (\AA^2) of schairerite at 600 K.

Atom	<i>x</i>	<i>y</i>	<i>z</i>	Occupancy	<i>U</i> (eq)
S1	2/3	1/3	0.35024(7)	S	0.0228(4)
S2	0	0	0.22912(9)	S	0.0306(4)
S3	2/3	1/3	0.07692(7)	S	0.0244(4)
S4	0	0	1/2	S	0.0296(5)
Cl1	0	0	0	Cl	0.0623(9)
Na1	1/2	1/2	1/2	Na	0.0442(6)
Na2	0.18109(14)	0.3622(3)	0.36493(9)	Na	0.0403(5)
Na3	0.48619(13)	0.51381(13)	0.22029(8)	Na	0.0404(5)
Na4	0.18060(16)	0.3612(3)	0.08183(11)	Na	0.0542(6)
F1	1/3	2/3	0.4488(2)	F	0.0401(9)
F2	1/3	2/3	0.29469(14)	F	0.0339(8)
F3	1/3	2/3	0.1473(2)	F	0.0438(10)
O1	0.5540(2)	0.4460(2)	0.37514(16)	O	0.0443(7)
O2	2/3	1/3	0.2756(3)	O	0.0524(14)
O3	0	0	0.1483(6)	0.5O	0.074(3)
O4	0.7767(14)	0.8884(7)	0.2076(4)	0.5O	0.0451(17)
O5	0.7745(16)	0.8873(8)	0.2438(5)	0.5O	0.067(3)
O6	0	0	0.3090(6)	0.5O	0.074(3)
O7	2/3	1/3	0.0042(3)	O	0.074(2)
O8	0.465(5)	0.233(2)	0.1174(17)	0.1O	0.054(8)
O9	0.5547(3)	0.1094(6)	0.1024(2)	0.9O	0.0655(11)
O10	0	0	0.4197(5)	0.5O	0.064(3)
O11	−0.1142(7)	−0.2283(13)	0.5131(6)	0.4O	0.064(2)
O12	−0.099(3)	−0.197(6)	0.471(2)	0.1O	0.064(2)

Table 5. Selected bond lengths (Å) of galeite at 300 K.

S1—O2	1.475(3)	S6—O1	1.476(3)(3×)
—O3	1.472(2)(2×)	—O14	1.477(2)
—O1	1.478(3)	<S6—O>	1.476
<S1—O>	1.474	S7—O16	1.471(2)(3×)
S2—O4	1.480(4)	—O17	1.469(4)
—O5	1.470(2)(3×)	<S7—O>	1.471
<S2—O>	1.473	Cl1—Na11	2.7035(15)(2×)
S3—O6	1.4729(19)(3×)	—Na1	2.7035(15)
—O7	1.473(4)	—Na9	2.8595(18)(3×)
<S3—O>	1.473	<Cl1—Na>	2.781
S4—O9	1.476(2)(2×)	Cl2—Na2	2.857(2)(3×)
—O8	1.474(2)	—Na10	2.6789(18)(3×)
—O10	1.476(4)	<Cl2—Na>	2.768
<S4—O>	1.475	F1—Na3	2.289(2)(2×)
S5—O11	1.471(5)	—Na1	2.360(2)(2×)
—O12	1.472(3)(3×)	—Na4	2.338(3)
<S5—O>	1.472	—Na2	2.349(3)
		<F1—Na>	2.330
F2—Na3	2.295(2)(2×)	Na1—O3	2.336(2)
—Na6	2.419(2)(2×)	—O1	2.388(2)
—Na4	2.241(3)	—O6	2.439(2)
—Na5	2.610(3)	—O15	2.464(3)
<F2—Na>	2.380		
F3—Na5	2.228(3)	Na2—O15	2.432(3)
—Na6	2.267(2)(2×)	—O3	2.434(2)(2×)
—Na7	2.418(2)	—O4	2.442(3)
—Na8	2.327(2)(2×)		
<F3—Na>	2.306	Na3—O3	2.404(3)
F4—Na10	2.230(3)	—O5	2.422(2)
—Na7	2.260(3)	—O6	2.428(2)
—Na9	2.299(2)(2×)	—O9	2.486(3)
—Na8	2.309(2)(2×)		
<F4—Na>	2.284	Na4—O6	2.421(2)(2×)
Na5—O5	2.343(3)	—O1	2.435(4)
—O9	2.374(2)(2×)	—O8	2.490(4)
—O11	2.445(3)		
		Na6—O8	2.380(2)
Na7—O16	2.409(2)(2×)	—O9	2.392(2)
—O10	2.489(3)	—O16	2.411(3)
—O13	2.505(4)	—O7	2.431(2)
Na9—O13	2.393(2)		
—O2	2.419(3)	Na8—O12	2.385(2)
—O14	2.437(2)	—O10	2.415(2)
—O17	2.488(2)	—O16	2.420(2)
		—O14	2.464(3)
Na10—O14	2.362(2)(2×)		
—O12	2.548(4)		
—O2	2.477(3)		

Table 6. Selected bond lengths (Å) of schairerite at 300 K.

S1—O2	1.454(4)(3×)	S6—O14	1.434(8)
—O1	1.501(9)	—O13	1.470(7)
<S1—O>	1.466	—O12	1.477(5)(2×)
S2—O3	1.472(6)(3×)	<S6—O>	1.465
—O4	1.480(1)	S7—O16	1.470(4)(3×)
<S2—O>	1.474	—O15	1.489(10)
S3—O6	1.455(4)(3×)	<S7—O>	1.475
—O7	1.504(9)	S8—O19	1.471(6)
<S3—O>	1.467	—O18	1.479(4)(2×)
S4—O9	1.482(7)	—O17	1.498(7)
—O7	1.482(4)(2×)	<S8—O>	1.481
—O8	1.480(6)	S9—O21	1.459(6)
<S4—O>	1.482	—O22	1.466(4)(2×)
S5—O10	1.458(6)(3×)	—O20	1.470(8)
—O11	1.469(6)	<S9—O>	1.465
<S5—O>	1.461	F1—Na3	2.243(6)
Cl1—Na8	2.661(4)(3×)	—Na1	2.279(5)(2×)
—Na13	2.848(5)(3×)	—Na11	2.418(5)(2×)
<Cl1—Na>	2.754	—Na14	2.588(7)
Cl2—Na9	2.687(5)(3×)	<F1—Na>	2.312
—Na7	2.827(6)(3×)	F2—Na1	2.234(4)(2×)
<Cl1—Na>	2.757	—Na3	2.281(6)
F3—Na4	2.279(5)(2×)	—Na2	2.339(6)
—Na2	2.287(7)	—Na4	2.508(5)(2×)
—Na5	2.294(7)	<F2—Na>	2.351
—Na6	2.374(5)(2×)	F4—Na8	2.225(5)(2×)
<F3—Na>	2.315	—Na6	2.274(5)(2×)
F5—Na9	2.231(7)	—Na7	2.274(7)
—Na12	2.275(7)	—Na5	2.317(6)
—Na13	2.284(5)(2×)	<F4—Na>	2.265
—Na10	2.237(5)(2×)	F6—Na14	2.231(6)
<F5—Na>	2.258	—Na11	2.255(4)(2×)
Na1—O3	2.415(5)	—Na10	2.331(5)(2×)
—O2	2.426(5)	—Na12	2.419(6)
—O22	2.466(6)	<F6—Na>	2.303
—O7	2.499(7)		
		Na4—O7	2.347(5)
Na2—O7	2.386(4)(2×)	—O8	2.373(5)
—O10	2.432(9)	—O2	2.420(6)
—O4	2.425(6)	—O5	2.447(5)
Na3—O2	2.423(3)(2×)	Na5—O6	2.385(4)(2×)
—O21	2.450(9)	—O13	2.403(9)
—O8	2.508(9)	—O9	2.396(8)
Na6—O6	2.382(5)	Na7—O12	2.426(5)(2×)
—O10	2.408(5)	—O17	2.457(8)
—O12	2.439(7)	—O11	2.471(7)
—O9	2.453(5)		
		Na9—O18	2.376(5)(2×)
Na8—O12	2.367(5)	—O14	2.474(8)
—O13	2.408(5)	—O24	2.623(9)
—O17	2.466(6)		
—O16	2.580(7)	Na10—O24	2.375(5)
		—O20	2.414(5)
Na11—O21	2.398(5)	—O16	2.418(4)
—O16	2.395(6)	—O18	2.435(7)
—O22	2.404(5)		
—O1	2.430(5)	Na12—O16	2.403(4)
		—O19	2.476(9)
Na13—O19	2.399(5)	—O20	2.496(8)
—O18	2.435(5)		
—O14	2.474(6)	Na14—O22	2.377(4)(2×)
—O15	2.512(6)	—O3	2.397(8)
		—O23	2.430(7)

Table 7. Selected bond lengths (Å) of schairerite at 600 K.

S1—O2	1.462(5)	S4—O11	1.417(8)(6×)
—O1	1.464(3)(3×)	—O13	1.41(2)(6×)
<S1—O>	1.464	<S4—O>	1.413
S2—O5	1.414(9)(3×)	Cl1—Na4	2.732(2)(6×)
—O4	1.430(8)(3×)	<Cl1—Na>	2.732
—O6	1.56(1)	F1—Na1	2.275(2)(3×)
—O2	1.57(1)	Na2	2.486(3)(3×)
<S2—O>	1.458	<F1—Na>	2.381
S3—O7	1.425(6)	F2—Na2	2.318(3)(3×)
—O9	1.460(4)(3×)	—Na3	2.373(3)(3×)
—O8	1.47(2)(3×)	<F2—Na>	2.346
<S3—O>	1.459	F3—Na4	2.268(3)(3×)
Na1—O11	2.445(6)(4×)	—Na3	2.356(3)(3×)
—O1	2.534(3)(2×)	<F3—Na>	2.312
—O12	2.58(2)(4×)	Na2—O1	2.405(2)(2×)
		—O10	2.470(5)
Na3—O4	2.421(6)(2×)	—O6	2.474(6)
—O5	2.439(7)(2×)	—O5	2.515(9)
—O9	2.459(4)	—O11	2.53(1)
—O2	2.462(3)		
		Na4—O9	2.437(3)(2×)
		—O7	2.518(4)
		—O3	2.570(6)
		—O4	2.606(7)

2.3. Raman Spectra

The Raman spectra of galeite and schairerite were studied using a Horiba Jobin-Yvon LabRam HR 800 system operated in the range of 70–4000 cm^{−1} (a solid-state laser with $\lambda = 532$ nm and a silicon standard was used, power on the sample was 8 mW, and 50× objective was employed). Samples were kept at room temperature and oriented randomly. The data accumulation time was from 2 to 10 s. The obtained spectra were visualized using OriginPro 2018 SR1 b9.5.1.195.

2.4. Structural Complexity Calculation

The structural complexity measures of galeite and both modifications of schairerite were calculated as the amounts of Shannon information per atom ($^{\text{str}}I_G$) and per unit cell ($^{\text{str}}I_{G,\text{total}}$) using the methodology discussed in [28,29] and the following equations:

$$I_G = \sum_{i=1}^K p_i \log_2 p_i \left(\frac{\text{bits}}{\text{atom}} \right) \quad (2)$$

$$I_{G,\text{total}} = -\nu \sum_{i=1}^K p_i \log_2 p_i (\text{bits}/\text{u.c.}) \quad (3)$$

Above, k is a multiplicity of a crystallographic orbit, p_i is a random choice probability for an atom from the i th crystallographic orbit, that is,

$$p_i = m_i / \nu, \quad (4)$$

where m_i is a multiplicity of a crystallographic orbit relative to the reduced unit cell and ν is the number of atoms in the reduced unit cell. TOPOSPro software was used for the calculations [30].

2.5. BVS for Na-Ion Transport

BVS maps were calculated for a preliminary assessment of possible Na-ion pathways. The BVS maps at various bond–valence mismatches $Z_i - \Sigma s_i$ ($Z_i = 1$ for Na⁺, $s_i = \exp[(R_0 - R)/b]$, where R_0 and b are empirical constants, R is the cation–anion distance,

and Σs_i is BVS) were calculated using the BondStr program [31] for Na^+ sites in grids with steps of Δx , Δy , and $\Delta z = 0.1 \text{ \AA}$ in the unit cell with the fixed sites of other atoms. The calculated data were visualized using VESTA software [27].

3. Results

3.1. Raman Spectra

The Raman spectra of galeite and schairerite are shown in Figure 5. They are very similar to each other and are in good agreement with the spectra reported in the RRUFF database for galeite (data on schairerite are not available) [32]. The main bands of both spectra correspond to symmetric and asymmetric vibrations of SO_4 tetrahedra: the most intense bands at 998 cm^{-1} can be attributed to symmetric S-O stretching vibrations (ν_1), and the middle-intensity bands at 637 and the shoulder at 624 cm^{-1} for galeite are in-plane bending vibrations of SO_4^{2-} groups (ν_4), whereas the low-intensity bands at 469 cm^{-1} for both minerals and at 459 cm^{-1} for schairerite are attributed to out-of-plane vibrations (ν_2); finally, the bands in the $1100\text{--}1200 \text{ cm}^{-1}$ region can be attributed to anti-symmetric stretching vibrations. The bands at 221 cm^{-1} are connected to lattice vibrations [33].

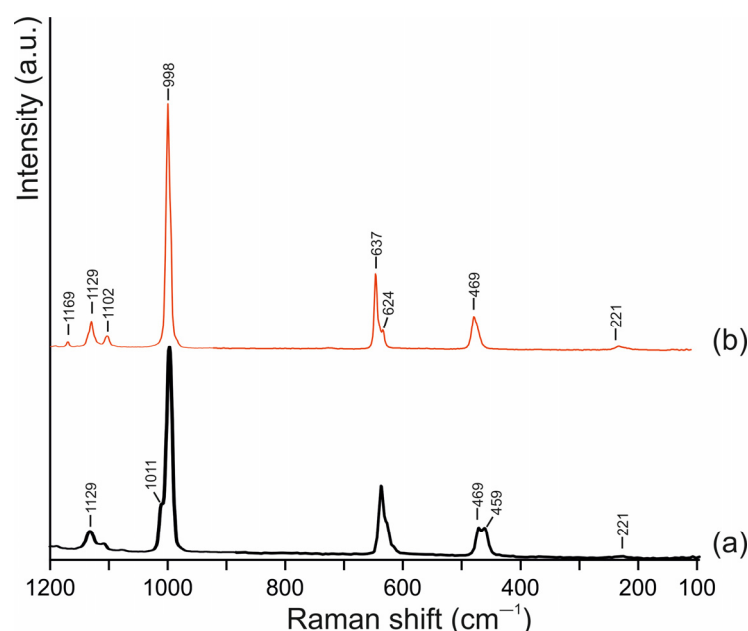


Figure 5. Raman spectra of schairerite (a) and galeite (b).

3.2. Structure Description

The crystal structure refinement data at 300 K are in good agreement with the data obtained previously by Fanfani and co-authors [17,19]. As mentioned above, galeite and schairerite have the same $P31m$ space group and differ only in the value of the c parameter: $a = 12.1903(2)$, $c = 13.9454(2) \text{ \AA}$, and $V = 1794.69(6) \text{ \AA}^3$ ($R_1 = 0.0273$, 300 K) were obtained for galeite, and $a = 12.1859(3)$, $c = 19.3080(6) \text{ \AA}$, and $V = 2483.04(14) \text{ \AA}^3$ ($R_1 = 0.0334$, 300 K) were obtained for schairerite. The two minerals have similar topologies and, according to the authors of [17,18], can be described in terms of Na^+ ion layers located perpendicular to the c direction. The layers are similar but form different five- and seven-sheet sequences: BABAC for galeite and BABACAC for schairerite. Each sheet can be considered a set of hexagons and triangles with centers corresponding to ternary axes and pseudo-axes. Sulfur atoms are located in these centers within the sheets, whereas chlorine and fluorine ions lie between the sheets with different interlayer distances (Figure 6a,b). The arrangement of Na ions is centrosymmetric in schairerite, which is not the case for galeite. According to Fanfani [17] and co-authors, the Na^+ ion coordination can be considered to be distorted octahedra

$\text{Na}(\text{OSO}_3)_{4 \times 2}$, with $X_2 = \text{F}_2$ or FCl . These octahedra share corners, edges, and faces, forming a three-dimensional framework with tetrahedral holes occupied by sulfur atoms.

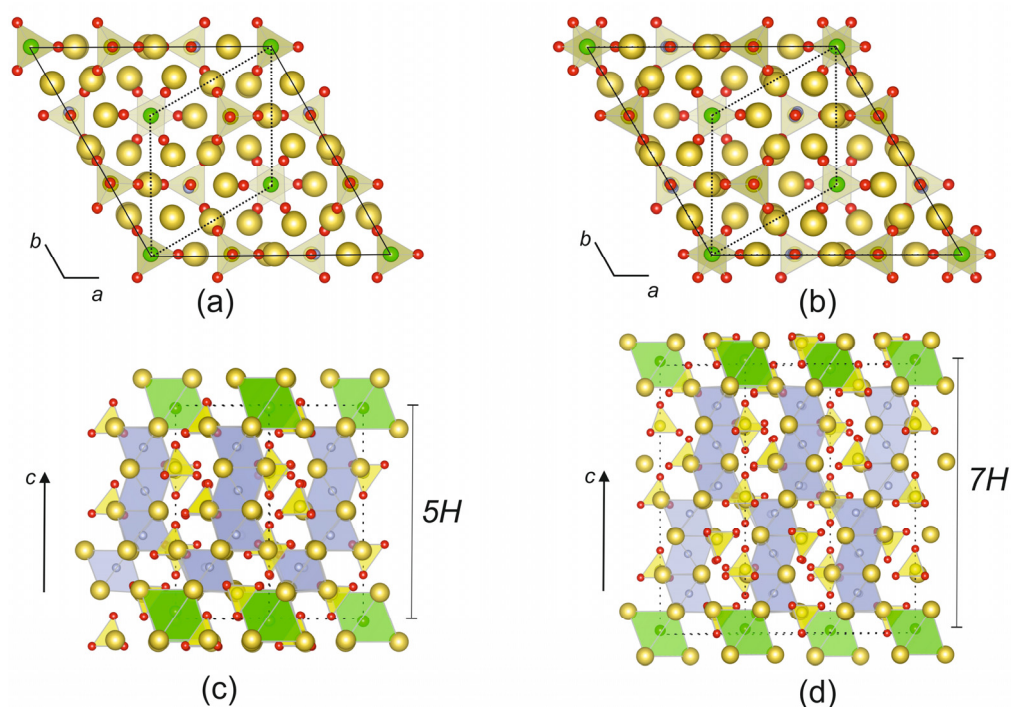


Figure 6. The crystal structures of galeite (a,c) and schairerite (b,d) presented as Na^+ layers and anion-centered polyhedra. Legend: Na atoms are yellow, O atoms are red, Cl atoms are shown in green, and F atoms are gray. Sulfur tetrahedra are light yellow (a,b) and yellow (c,d), FNa_6 octahedra are gray, and ClNa_6 octahedra are light green. Subcells are indicated by the dotted lines.

Krivovichev [5] proposed describing the crystal structures of galeite and schairerite based upon antiperovskite anion-centered frameworks. In this approach, the crystal structures of the minerals are based on alternating face- and corner-sharing fluorine- and chlorine-centered octahedra. The isolated (ClNa_6) octahedra have common vertices, with (FNa_6) octahedra forming three-dimensional frameworks in both structures. The SO_4 tetrahedra are in the framework cavities, with one of the S-O bonds parallel to the c axis (Figure 6c,d). The average bond lengths in the sulfate tetrahedra have standard values and deviations. In general, the crystal structures of schairerite and galeite are fully ordered at 300 K and can be attributed to $5H$ (galeite) and $7H$ (schairerite) antiperovskite polytypes, respectively.

3.3. HT-Modification of Schairerite

The crystal structure of HT-schairerite was refined at 600, 650, and 700 K. It has the same topology and is based on a framework consisting of anion-centered octahedra. The HT-modification has the centrosymmetric space group $P-3m1$, with $a = 7.0714(2)$ Å and the c parameter being almost identical to that of the LT phase ($c = 19.5972(7)$ Å). This coincides with the pseudo-cell described previously by Fanfani and co-authors [18]. In contrast to the LT-modification, there were four non-equivalent S and Na sites, three F sites, and one Cl site. The main difference between the LT and HT modifications lies in the orientation of oxygen in the sulfate tetrahedra. During the refinement, the presence of additional electron-density peaks near the S site was observed and refined as low-occupied O sites with S-O distances ranging from 1.41 to 1.57 Å and site occupancy factors ranging from 0.1 to 0.9 (Tables 4 and 7, Figure 7). A detailed inspection of the Fourier difference electron-density maps constructed from the data obtained at different temperatures showed the appearance of residual peaks around threefold axes, even at 350 K. The intensity of the additional peaks

in schairerite rose with temperature, whereas such a tendency was not observed for galeite up to 475 K.

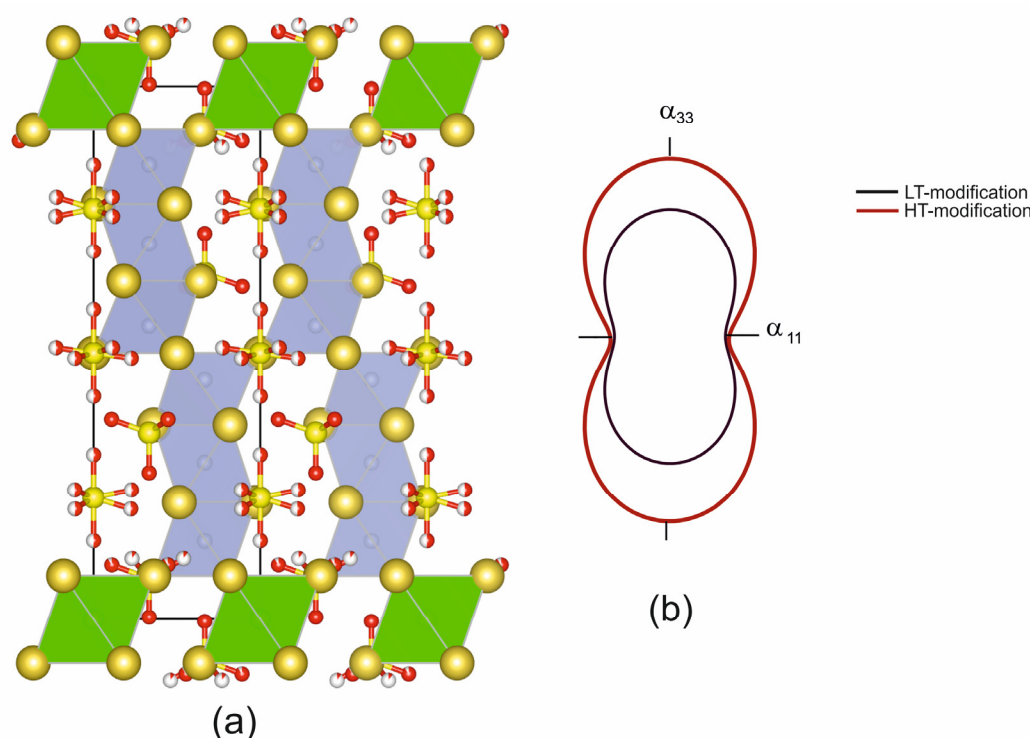


Figure 7. The crystal structure of HT-modification of schairerite (a) and the orientation of the section of the figure of thermal expansion coefficients (b) for the HT and LT phases. Projection on the ac plane. Legend is the same as that in Figure 6.

3.4. Thermal Behavior

The temperature dependencies of the unit-cell parameters for galeite were approximated using the following equations ($\times 10^6 \text{ }^\circ\text{C}^{-1}$): $a = 12.1827 + 0.2 \times 10^{-3} T$, $R^2 = 0.9860$; $c = 13.9333 + 0.4 \times 10^{-3} T + 0.6 \times 10^{-6} T^2$, $R^2 = 0.9992$; and $V = 1789.87 + 0.15 \times T$, $R^2 = 0.9946$. The parameters increased almost uniformly in the range of 300–500 K.

Similar equations for schairerite were derived separately for the LT and HT phases using linear and second-order (for the c parameter) approximations: $a = 12.18128 + 0.2 \times 10^{-3} T$, $R^2 = 0.9946$; $c = 19.2893 + 0.7 \times 10^{-3} T + 0.6 \times 10^{-6} T^2$, $R^2 = 0.9992$; $V = 2478.17 + 0.20 \times T$, $R^2 = 0.9946$ (LT-schairerite); $a = 7.031 + 0.1 \times 10^{-3} T$, $R^2 = 0.9986$; $c = 19.1289 + 0.2 \times 10^{-2} T - 0.1 \times 10^{-5} T^2$, $R^2 = 0.9996$; and $V = 823.91 + 0.09 \times T$, $R^2 = 0.9982$ (HT-schairerite). The unit-cell parameters for the HT modification were recalculated in the LT modification setting for the comparison and representation of the data in the same graph. The transition accompanied by the changes in parameters is clearly visible (Figure 7b, 8).

The calculation of thermal expansion coefficients indicates the same tendency of thermal expansion for galeite and schairerite, which almost did not change with an increasing temperature ($\times 10^6 \text{ }^\circ\text{C}^{-1}$): $\alpha_{11} = 19.4(9)$, $\alpha_{33} = 42.9(1)$, $\alpha_V = 81.8(2)$ (galeite, 25 $^\circ\text{C}$); $\alpha_{11} = 18.5(1)$, $\alpha_{33} = 42.4(1)$, $\alpha_V = 79.3(2)$ (schairerite, 25 $^\circ\text{C}$); $\alpha_{11} = 20.5(5)$, $\alpha_{33} = 63.4(2)$, and $\alpha_V = 104.3(3)$ (schairerite, 325 $^\circ\text{C}$). The $\alpha_{\max}/\alpha_{\min}$ values were almost the same for galeite (2.21) and LT-schairerite (2.29) but slightly increased following the HT-modification of schairerite (3.09). The strongest thermal expansion was observed parallel to the modules of face-sharing anion-centered octahedra oriented along the c axis (Figures 7 and 8). This kind of thermal expansion is typical for compounds with antiperovskite units and has been explained in our previous works [12,13]. The value and direction of thermal expansion depends heavily on the polyhedrons' rigidity and their location and linkage in the crystal structure. From this point of view, the modules of face-sharing F-centered octahedra are

apparently responsible for the expansion, which has been interpreted as being governed by the repulsion of F^- anions across the triangular faces shared between the adjacent octahedra, i.e., parallel to the c axis [19,21].

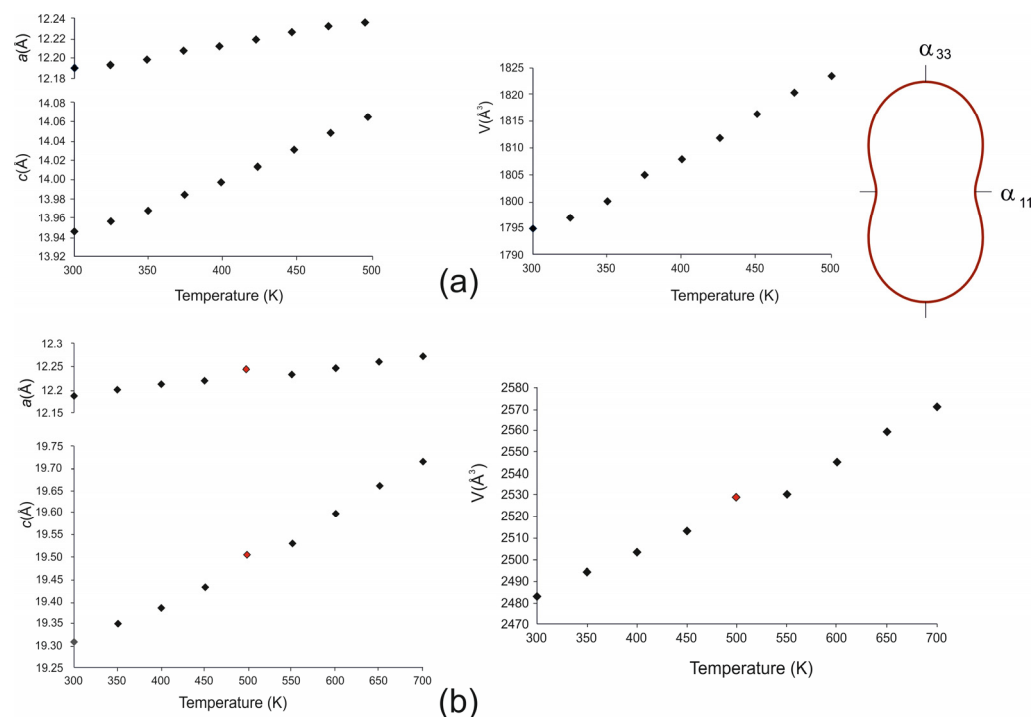


Figure 8. The dependencies of the unit cell parameters of galeite and the section of the figure of thermal expansion coefficients (a); the dependence of the unit cell parameters of schairerite shown in low-temperature modification setting (b).

3.5. Structural Complexity

The structural complexity of galeite and both modifications of schairerite (300 and 600 K) was measured using Shannon information per atom and Shannon information per unit cell (Table 8). The differences and peculiarities are discussed in Section 4.

Table 8. The structural complexity of galeite and both modifications of schairerite including per atom (I_G bits/atom) and for unit cell ($I_{G,total}$ bits/cell).

	ν	Space Group	I_G , Bits/Atom	$I_{G,total}$, Bits/Cell
Galeite	135	$P31m$	5.149	695.175
LT-schairerite	189	$P31m$	5.635	1064.990
HT-schairerite	63	$P-3m1$	4.075	256.755

3.6. Sodium-Ion Migration in Galeite and Schairerite

Using our structural data for galeite and schairerite, we created BVS maps and predicted the probability of the migration of Na^+ ions (Figure 9). Our calculations show the probability of Na^+ migration in the crystal structure of galeite, which can occur in the ab plane at 1.45 eV, and along the c direction between two layers only at 2.06 eV. The migration of sodium ions is possible only with diffusion along the c axis. There are two pathways, considering a percolation energy of 2.06 eV, that are not connected with each other. The first path involves Na(1), Na(5), Na(7), Na(8), and Na(9) sites, whereas the second path involves Na(2), Na(3), Na(4), Na(6), and Na(10) sites.

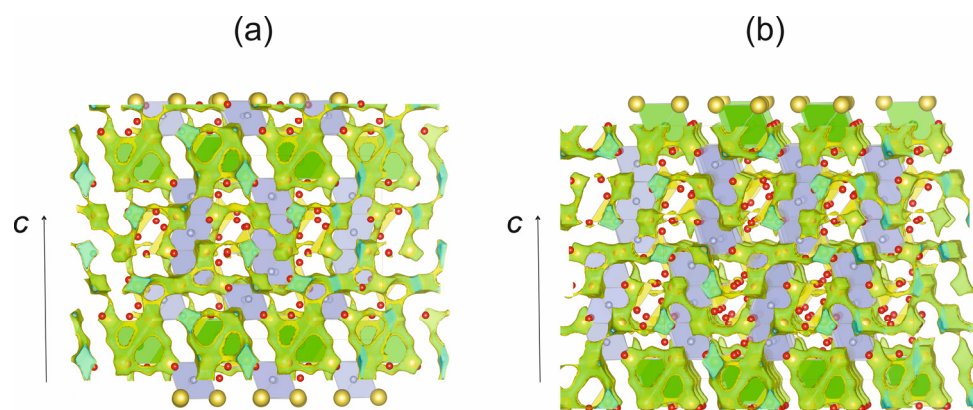


Figure 9. The BVS map isosurfaces (0.10) for sodium ions in galeite (a) and the BVS map isosurfaces (0.15) for sodium ions in schairerite (b). Legend is the same as in Figure 6.

The calculations also indicate a probability of Na^+ migration in the crystal structure of schairerite. In the ab plane, this migration occurs at 1.53 eV, and it occurs at 2.21 eV along the c direction. There are no three-dimensional Na-ion migration paths in this crystal structure at room temperature. Analysis of the calculated data reveals three independent pathways of Na-ion migration in the crystal structure. All of them are in the ab plane, with ion diffusion between some layers. The first path involves the Na(1), Na(3), and Na(10) sites; the second involves the Na(4), Na(5), and Na(6) sites; and the third involves the Na(8), Na(10), Na(12), Na(13), and Na(14) sites.

4. Discussion

The positional disorder of SO_4 tetrahedra under increasing temperature did not allow for the informative and reliable analysis of the S-O bond lengths for the crystal structures of galeite and schairerite. Nonetheless, it is possible to draw some conclusions concerning the bonds in the anion-centered octahedra. In galeite, most of the Na-F bonds elongate with increasing temperature. Three of four F-centered polyhedra form trimers of face-sharing octahedra (F2Na_6 , F3Na_6 , and F4Na_6), whereas F1Na_6 octahedra link adjacent trimers via corner sharing (Figure 6c). The F2Na_6 octahedra demonstrate the largest increase in volume, from 16.2570 \AA^3 (300 K) to 16.7799 \AA^3 (500 K) (approximately 3.2%), which can be explained by their central position in the trimer. The volumetric expansion of two other octahedra was less than 2% (F2Na_6 —1.8%; F3Na_6 —1.9%). The F1-Na3 and F1-Na4 bonds related to the extra-trimer octahedra remained unchanged within the errors of measurement. The relative increase or decrease in the Na-Cl bonds is insignificant: the maximal elongation of bonds as well as polyhedra volume change values were less than 1% (Supplementary Materials).

In contrast to galeite, all the F-centered octahedra in schairerite are involved in the construction of trimers. The Na-F bonds enlarged when heated, but, for some bonds, the changes were within the errors of measurement (F3-Na_6 , F5-Na_9 , and F6-Na_{12}). In the case of the HT-modification of schairerite, the relative volumetric expansion of the fluorine-centered octahedra volume was almost uniform (1.76–1.84%). The tendency of the changes in the Na-Cl bonds is similar to that of galeite. For instance, the relative decrease of Cl1-Na13 bond ($\Delta = -0.04$) was nearly 1.2%.

As mentioned above, the maximal thermal expansion in all the structures was observed in the direction of the elongation of face-sharing octahedral anion-centered modules. The conducted bond analysis confirms that the temperature-induced distortions of face-sharing F-centered octahedra contribute the most to the anisotropy of thermal expansion compared to the similar contribution made by the Cl-centered octahedra.

The phase transition of schairerite has many similarities with the transition observed for the synthetic analogue of kogarkoite, $\text{Na}_3\text{SO}_4\text{F}$ [12]. Despite their differences in symmetry (kogarkoite is monoclinic; $P2_1/m$, $a = 18.065(3)$, $b = 6.958(1)$, $c = 11.446(1) \text{ \AA}$, and $\beta = 107.711^\circ$), both minerals contain corner-sharing trimers of F-centered octahedra, which

form a continuous network in kogarkoite and are «cut out» by the isolated Cl-centered octahedra in schairerite. The reversible transitions in these minerals are accompanied by the strong positional disorder of SO_4 tetrahedra. In kogarkoite, the existence of a long-range order region between the low- and high-temperature modifications was assumed due to the strong libration effects observed. In the case of schairerite, an intermediate phase, which was most likely connected to the overlapping of the domains, was observed.

The nature of subcells in the crystal structures of schairerite and galeite was discussed in [18]. The authors pointed out that “the different orientation of sulfate groups along the threefold axes is the main reason justifying a description of the crystal structure of schairerite in the larger cell” (i.e., the unit cell of the LT-modification). This statement is clearly confirmed by our research, where the increasing positional disorder of SO_4 tetrahedra under elevated temperatures triggered the cell–subcell phase transition.

Galeite and schairerite differ essentially in their structural complexity and correspond to different complexity groups [28]: galeite is complex (500–1000 bits), whereas schairerite (>1000 bits) is very complex. According to Krivovichev [29], borates and sulfates are the most complex compounds between the O-bearing compounds, and this observation had been confirmed herein. The complexities of the LT- and HT-polymorphs of schairerite are consistent with the general observations regarding structures with positional disorder: complexity decreases with increasing temperature, and the polymorphs with lower complexity have lower physical density [29].

The lower melting point of galeite is apparently connected to its lower F/Cl ratio compared to schairerite, and its non-symmetric arrangement of sodium ions in contrast to schairerite is probably the main reason for the absence of an obvious phase transition despite the close similarity of the two crystal structures. However, this topic requires more detailed research.

In this work, we have also demonstrated that sodium diffusion is possible in both galeite and schairerite at room temperature. The potential for ionic conduction for one type of ion depends on bond lengths and valence forces in different crystallographic directions, and that is why there are differences in Na movement.

Our analysis of migration pathways shows that migration is possible if the percolation energies are 2.06 and 2.21 eV, respectively, and this is due to the low probability of direct Na–Na migration between some layers in the crystal structures.

Supplementary Materials: The following supporting information can be downloaded at: <https://www.mdpi.com/article/10.3390/sym15101871/s1>.

Author Contributions: Conceptualization, M.S.A., S.V.K. and A.A.Z.; methodology, M.S.A. and A.A.Z.; validation, S.V.K. and M.S.A.; formal analysis, A.P.S., M.S.A., V.N.B. and A.V.K.; investigation, M.S.A. and A.P.S.; writing—original draft preparation, M.S.A. and A.P.S.; writing—review and editing, S.V.K., A.A.Z., A.V.K., A.P.S. and V.N.B.; visualization, M.S.A. and A.P.S.; supervision, project administration and funding acquisition, M.S.A. All authors have read and agreed to the published version of the manuscript.

Funding: This research was funded by the Russian Science Foundation, grant No 22-77-00042, <https://rscf.ru/en/project/22-77-00042/> (accessed on 26 August 2023).

Data Availability Statement: Not applicable.

Acknowledgments: The X-ray diffraction studies were performed in the X-ray Diffraction Resource Centre of St. Petersburg State University. The spectroscopic studies were performed in the “Geo-model” Resource Centre of St. Petersburg State University.

Conflicts of Interest: The authors declare no conflict of interest.

References

1. Pabst, A.D.; Sharp, W.N. Kogarkoite, a new natural phase in the system Na_2SO_4 – NaF – NaCl . *Am. Min.* **1973**, *58*, 116–127.
2. Fanfani, L.; Giuseppetti, G.; Tadini, C.; Zanazzi, P.F. The crystal structure of kogarkoite, $\text{Na}_3\text{SO}_4\text{F}$. *Mineral. Mag.* **1980**, *43*, 753–759. [\[CrossRef\]](#)

3. Hidden, W.E.; Mackintosh, J.B. On a new sodium sulphato-chlorine, sulphohalite. *Am. J. Sci.* **1888**, *136*, 463–464. [CrossRef]
4. Pabst, A.D. The crystal structure of sulphohalite. *Z. Kristallogr.* **1934**, *89*, 514–517. [CrossRef]
5. Krivovichev, S.V. Minerals with antiperovskite structure: A review. *Z. Kristallogr.* **2008**, *223*, 109–113. [CrossRef]
6. Hoffmann, N.; Cerqueira, T.F.T.; Schmidt, J.; Marques, M.A.L. Superconductivity in antiperovskites. *N. Comput. Mater.* **2022**, *8*, 150. [CrossRef]
7. Dawson, J.A.; Famprikis, T.; Johnston, K.E. Anti-perovskites for solid state batteries: Recent developments, current challenges and future prospects. *J. Mater. Chem.* **2021**, *9*, 18746–18772. [CrossRef]
8. Takenaka, K.; Asano, K.; Misawa, M.; Takagi, H. Negative thermal expansion in Ge-free antiperovskite manganese nitrides: Tin-doping effect. *Appl. Phys. Lett.* **2008**, *92*, 011927. [CrossRef]
9. Shan, L.; Feng, S.; Liu, X.; Kan, X. Superconductivity and magnetic properties in antiperovskite nitride ZnNNi_3 . *Phys. C Supercond.* **2022**, *603*, 1354158. [CrossRef]
10. Sreedevi, P.D.; Vidya, R.; Ravindran, P. Antiperovskite materials as promising candidates for efficient tandem photovoltaics: First-principles investigation. *Mater. Sci. Semicond. Process.* **2022**, *147*, 106727. [CrossRef]
11. Nagpure, I.; Dhoble, S.J.; Godbole, S.V.; Bhide, M.K.; Pode, R.B. Eu^{3+} luminescence in $\text{Na}_3\text{SO}_4\text{F}$ and NaMgSO_4F halosulphate phosphor for mercury-free lamps. *Indian J. Eng. Mater. Sci.* **2009**, *16*, 181–184.
12. Avdontceva, M.S.; Zolotarev, A.A.; Krivovichev, S.V. Order-disorder phase transition in the antiperovskite-type structure of synthetic kogarkoite, $\text{Na}_3\text{SO}_4\text{F}$. *J. Solid State Chem.* **2015**, *231*, 42–46. [CrossRef]
13. Avdontceva, M.S.; Krzhizhanovskaya, M.G.; Krivovichev, S.V.; Yakovenchuk, V.N. High-temperature order-disorder phase transition in nacaphite, $\text{Na}_2\text{CaPO}_4\text{F}$. *Phys. Chem. Min.* **2015**, *42*, 671–676. [CrossRef]
14. Fleisher, M. New mineral names. *Am. Min.* **1956**, *41*, 671–674.
15. Pabst, A.; Sawyer, D.L.; Switzer, G. Galeite and related phases in the system $\text{Na}_2\text{SO}_4\text{--NaF--NaCl}$. *Am. Min.* **1963**, *48*, 485–510.
16. Foshag, W.F. Schairerite, a new mineral from Searles Lake, California. *Am. Min.* **1931**, *16*, 133–139.
17. Pabst, A.; Sawyer, D.L.; Switzer, G. Galeite, a new mineral from Searles Lake, California. *Geol. Soc. Am. Bull.* **1955**, *66*, 1658–1659.
18. Fanfani, L.; Nunzi, A.; Zanazzi, A.R. The crystal structure of galeite, $\text{Na}_{15}(\text{SO}_4)_5\text{F}_4\text{Cl}$. *Mineral. Mag.* **1975**, *40*, 357–361. [CrossRef]
19. Fanfani, L.; Nunzi, A.; Zanazzi, A.R.; Sabelli, C. The crystal structure of schairerite and its relationship to sulphohalite. *Mineral. Mag.* **1975**, *40*, 131–139. [CrossRef]
20. Avdontceva, M.; Krivovichev, S.; Yakovenchuk, V. Natrophosphate, Arctic Mineral and Nuclear Waste Phase: Structure Refinements and Chemical Variability. *Minerals* **2021**, *11*, 186. [CrossRef]
21. Avdontceva, M.S.; Krzhizhanovskaya, M.G.; Krivovichev, S.V.; Zolotarev, A.A.; Yakovenchuk, V.N. Polymorphism of $\text{Na}_2\text{CaPO}_4\text{F}$: Crystal structures, thermal stability and structural complexity. *J. Solid State Chem.* **2023**, *319*, 123779. [CrossRef]
22. CRYALISPRO Software System, version 1.171.39.44; Rigaku Oxford Diffraction: Oxford, UK, 2015.
23. Sheldrick, G.M. Crystal structure refinement with SHELXL. *Acta Crystallogr. Struct. Chem.* **2015**, *71*, 3–8. [CrossRef] [PubMed]
24. Dolomanov, O.V.; Bourhis, L.J.; Gildea, R.J.; Howard, J.A.K.; Puschmann, H. OLEX2: A complete structure solution, refinement and analysis program. *Appl. Crystallogr.* **2009**, *42*, 339–341. [CrossRef]
25. Downs, R.T. Analysis of harmonic displacement factors. *Rev. Mineral. Geochem.* **2000**, *41*, 61–187. [CrossRef]
26. Bubnova, R.S.; Firsova, V.A.; Filatov, S.K. Software for determining the thermal expansion tensor and the graphic representation of its characteristic surface (Theta to Tensor-TTT). *Glass Phys. Chem.* **2013**, *39*, 347–350. [CrossRef]
27. Momma, K.; Izumi, F. VESTA 3 for three-dimensional visualization of crystal, volumetric and morphology data. *J. Appl. Crystallogr.* **2011**, *44*, 1272–1276. [CrossRef]
28. Krivovichev, S.V. Structural complexity of minerals: Information storage and processing in the mineral world. *Miner. Mag.* **2013**, *77*, 275–326. [CrossRef]
29. Krivovichev, S.V.; Krivovichev, V.G.; Hazen, R.M.; Aksenov, S.M.; Avdontceva, M.S.; Banaru, A.M.; Gorelova, L.A.; Ismagilova, R.M.; Korniyakov, I.V.; Kuporev, I.V.; et al. Structural and Chemical Complexity of Minerals: An Update. *Mineral. Mag.* **2022**, *86*, 183–204. [CrossRef]
30. Blatov, V.A.; Shevchenko, A.P.; Proserpio, D.M. Applied topological analysis of crystal structures with the program package ToposPro. *Cryst. Growth Des.* **2014**, *14*, 3576–3586. [CrossRef]
31. Rodríguez-Carvajal, J. The Program BondStr and Its GUI GBondStr. 2004. Available online: https://www.ill.eu/sites/fullprof/php/programsdcceb.html?pagina=Bond_Str (accessed on 23 September 2023).
32. Lafuente, B.; Downs, R.T.; Yang, H.; Stone, N. The power of databases: The RRUFF project. In *Highlights in Mineralogical Crystallography*; Armbruster, T., Danisi, R.M., Eds.; W. De Gruyter: Berlin, Germany, 2015; pp. 1–30.
33. Frezzotti, M.L.; Tecce, F.; Casagli, A. Raman spectroscopy for fluid inclusion analysis. *J. Geochem. Explor.* **2012**, *112*, 1–20. [CrossRef]

Disclaimer/Publisher’s Note: The statements, opinions and data contained in all publications are solely those of the individual author(s) and contributor(s) and not of MDPI and/or the editor(s). MDPI and/or the editor(s) disclaim responsibility for any injury to people or property resulting from any ideas, methods, instructions or products referred to in the content.